AGU PUBLICATIONS

JGR

Journal of Geophysical Research: Atmospheres

RESEARCH ARTICLE

10.1002/2014JD022314

Key Points:
- CLM simulations biased relative to GRACE and FLUXNET-MTE data sets
- Biases can be reduced by increasing soil resistance
- Dry surface layer formulation used to simulate soil resistances

Correspondence to:
S. C. Swenson,
swensosc@ucar.edu

Citation:
Swenson, S. C., and D. M. Lawrence (2014), Assessing a dry surface layer-based soil resistance parameterization for the Community Land Model using GRACE and FLUXNET-MTE data, *J. Geophys. Res. Atmos.*, *119*, 10,299–10,312, doi:10.1002/2014JD022314.

Received 14 JUL 2014
Accepted 18 AUG 2014
Accepted article online 21 AUG 2014
Published online 11 SEP 2014

Assessing a dry surface layer-based soil resistance parameterization for the Community Land Model using GRACE and FLUXNET-MTE data

S. C. Swenson[1] and D. M. Lawrence[1]

[1]Climate and Global Dynamics Division, National Center for Atmospheric Research, Boulder, Colorado, USA

Abstract The Community Land Model (CLM) exhibits biases in evapotranspiration (ET) and total water storage (TWS) in semiarid regions. The TWS seasonal cycle amplitude is too low, while evapotranspiration is too strong and variable. These biases are consistent with excessive soil evaporation when the canopy is sparse or absent, which reduces moisture inputs into the ground. Here we improve the simulation of soil evaporation by replacing CLM's existing empirical soil resistance parameterization with a more mechanistically based formulation in which soil evaporation is controlled by the rate of diffusion of water vapor through a dry surface layer (DSL). The thickness of the DSL is parameterized as a soil-type dependent function of top layer soil moisture. Soil resistances are calculated from the DSL thickness combined with a soil tortuosity factor. Compared to the existing CLM soil resistance parameterization, the DSL-based soil resistances for a given soil moisture value are generally larger, especially for moister soils. CLM simulations using the DSL-based soil resistance expression have reduced biases of ET relative to the FLUXNET-MTE (Model Tree Ensemble) data set and TWS relative to Gravity Recovery and Climate Experiment (GRACE) observations. Averaged over global semiarid regions, the CLM mean annual amplitude of TWS increases from 26.3 mm to 32.5 mm when the new soil resistance parameterization is used, in good agreement with the GRACE mean annual amplitude for these regions of 32.2 $\pm$ 2.1 mm. CLM mean annual ET, averaged over global semiarid regions, decreases from 27.8 mm/month to 23.5 mm/month, closer to the FLUXNET-MTE mean annual ET of 21.1 $\pm$ 0.9 mm/month. The seasonal amplitude of CLM ET also decreases, from 23.3 mm/month to 18.3 mm/month compared to 14.9 $\pm$ 1.1 mm/month for FLUXNET-MTE.

1. Introduction

A key task of a land model coupled in an Earth System modeling framework is the partitioning of moisture inputs from the atmosphere into evapotranspiration, runoff, and changes in land water storage. Each of these terms in the terrestrial water balance comprises in turn a set of individual processes. Evapotranspiration (ET), for example, can be decomposed into transpiration, canopy evaporation (i.e., the evaporation of water directly from the surface of vegetation), and soil evaporation. Spatial and temporal characteristics vary between these components; therefore, total ET must be partitioned properly to realistically simulate land-atmosphere interactions and their influence on climate. However, the separation of ET into its constituents is poorly constrained [*Lawrence et al.*, 2007]. Globally, satellite and model-derived estimates of ET partitioning span a wide range [*Miralles et al.*, 2011; *Jiménez et al.*, 2011; *Alton et al.*, 2009], from evaporation dominated (58% E/25% T) to transpiration dominated (7% E/80% T).

ET partitioning also influences the other terms in the water balance. The division of precipitation into evapotranspiration, runoff, and storage varies regionally due to climate, vegetation, soil characteristics, and topography. In some regions the combination of these factors results in a simplified water balance, in which one or more of the moisture fluxes contribute relatively little. For example, in semiarid regions, where vegetation is sparse and bare soil covers a significant fraction of the land surface, runoff is relatively small [*Haddeland et al.*, 2011]. The terrestrial moisture budget therefore is primarily a balance between changes in water storage and ET. Additionally, bare soil evaporation is the largest component of ET in semiarid regions, in contrast to more heavily vegetated regions in which transpiration is the dominant ET component [*Miralles et al.*, 2011]. A detailed examination of the water balance of semiarid regions can therefore provide insight into a model's ability to correctly simulate the contribution of soil evaporation to total ET.

In this study, we use observations of total water storage (TWS) from the Gravity Recovery and Climate Experiment (GRACE) satellite project [*Tapley et al.*, 2004] and evapotranspiration estimates from the FLUXNET-MTE (Model Tree Ensemble) data set [*Jung et al.*, 2009] to assess the simulation of the terrestrial water budget of a global land surface model. The Community Land Model (CLM) [*Lawrence et al.*, 2011] is the terrestrial component of the Community Earth System Model (CESM) [*Hurrell et al.*, 2013]; the technical description of the current version of CLM, version 4.5, can be found in *Oleson et al.* [2013]. Relative to CLM3.0, CLM4.0 showed significant improvement in the global simulation of total water storage relative to GRACE satellite observations [*Gent et al.*, 2011; *Lawrence et al.*, 2012], and the quality of the TWS simulation is maintained in CLM4.5. In some regions, however, large TWS biases still can be found in CLM4.5 simulations, particularly in semiarid regions. In these regions, we show that the amplitude of the TWS seasonal cycle is typically too low, by as much as 50% or more. This TWS bias can be largely attributed to problems with the simulation of evapotranspiration, specifically, soil evaporation, which appears to be too large and too variable when compared to FLUXNET-MTE ET data.

The existing CLM soil evaporation parameterization employs an empirical soil resistance function [*Sakaguchi and Zeng*, 2009; *Lawrence et al.*, 2011], which controls the magnitude of soil evaporation as a function of the uppermost soil layer soil moisture (section 4). Sensitivity experiments indicate that increasing soil resistance values relative to those in a standard CLM simulation reduces bare soil evaporation and increases net infiltration into the soil, leading to a larger seasonal cycle of soil moisture storage. With higher soil resistances, simulated TWS and ET both agree better with observations, suggesting that the existing CLM soil resistance formulation could be improved.

Laboratory and field studies of bare soil evaporation have been used to develop empirical relationships between soil resistance and near-surface soil moisture [e.g., *Kondo et al.*, 1990; *Sellers et al.*, 1992; *van de Griend and Owe*, 1994; *Sakaguchi and Zeng*, 2009]. Applying soil resistance parameterizations that directly link soil resistance to near-surface soil moisture in global land surface models can be problematic, however. Typically, the soil resistance-soil moisture relationships are site or soil specific, requiring extrapolation to the full range of soil types represented in global models such as CLM. In addition, directly parameterizing resistance as a function of soil moisture state ignores the physical processes responsible for controlling the transport of moisture through the near-surface soil.

Observations of bare soil undergoing evaporative drying indicate that the transition from atmosphere-controlled to soil-controlled evaporation occurs when a dry surface layer (DSL) forms near the soil surface [*Kondo and Saigusa*, 1994; *Yamanaka et al.*, 1997; *Liu et al.*, 2005; *Goss and Madliger*, 2007; *Shokri and Or*, 2011; *Deol et al.*, 2012; *Smits et al.*, 2012]. Within the DSL, soil moisture values are approximately air-dry (often less than half of wilting point), while below the DSL, soil moisture may be 3–4 times higher [*van de Griend and Owe*, 1994; *Kondo and Saigusa*, 1994]. At the bottom of the DSL, hydraulic connectivity is broken, and moisture transport transitions from mainly liquid phase flow to flow dominated by vapor diffusion [*Shokri et al.*, 2009]. When the DSL thickness is known, it can be combined with the diffusivity of water vapor through soil to estimate the soil evaporative resistance [*Deol et al.*, 2012; *Yamanaka et al.*, 1997].

Previously, two studies using CLM have calculated soil resistances based on the concept of vapor diffusion through a dry surface layer [*Sakaguchi and Zeng*, 2009; *Tang and Riley*, 2013]. When implemented within CLM, neither of the soil resistance parameterizations developed in the two studies had a significant impact on the TWS and ET biases observed in CLM simulations of semiarid regions.

In this study, we introduce in CLM a new dry surface layer parameterization, in which the thickness of the DSL is derived from the top model layer soil moisture. Diagnosing the DSL thickness more faithfully reflects the underlying process controlling soil evaporation. The effect of soil texture on the diffusivity of water vapor through soil is explicitly expressed by the use of a soil-type dependent tortuosity factor that describes the increase in diffusive path length caused by the soil matrix [*Moldrup et al.*, 2003]. Compared to the soil resistances in the standard version of CLM, as well as those derived by *Sakaguchi and Zeng* [2009] and *Tang and Riley* [2013], the soil resistances calculated from the DSL parameterization described in this study are significantly larger. Using the resulting soil resistances in CLM simulations simultaneously reduces the ET

and TWS biases in the semiarid study region. Globally, annual mean soil evaporation decreases and annual mean transpiration increases, making the CLM partitioning more similar to recent ET partitioning estimates [*Jasechko et al.*, 2013; *Miralles et al.*, 2011].

2. Model and Data Description

In this section we describe the land model used in this study, as well as the data sets used to assess the model simulations.

2.1. The Community Land Model

The Community Land Model (CLM) [*Lawrence et al.*, 2011] is the land component of the Community Earth System Model (CESM1) [*Hurrell et al.*, 2013]. CLM simulates the partitioning of mass and energy from the atmosphere, the redistribution of mass and energy within the land surface, and the export of fresh water to the oceans. To realistically simulate these interactions, CLM includes terrestrial hydrological processes such as interception of precipitation by the vegetation canopy, throughfall, infiltration, surface and subsurface runoff, snow and soil moisture evolution, evaporation from soil and vegetation, and transpiration [*Oleson et al.*, 2013].

In this study, CLM simulations are forced with atmospheric conditions for the period 1850–2012 from the CRUNCEP data set [*Viovy*, 2013]. The precipitation inputs available in the CRUNCEP data set are bias corrected for this study using merged satellite-gauge precipitation analyses from the Global Precipitation Climatology Project [*Huffman et al.*, 1997]. The spatial resolution of the simulations is 1.25° longitude × 0.9° latitude. Two simulations were run: a control simulation using CLM version 4.5 [*Oleson et al.*, 2013] and a simulation in which the soil evaporative resistance parameterization was replaced by the DSL-based parameterization (section 4.2).

2.2. GRACE Total Water Storage Data

The GRACE satellite project monitors the orbits of the twin GRACE satellites to produce monthly estimates of the Earth's gravity field [*Tapley et al.*, 2004]. Changes in the gravity field can be used to infer changes in total (vertically integrated) terrestrial water storage, and GRACE data have been used to make global estimates of TWS having a spatial resolution of a few hundred kilometers and greater [*Wahr et al.*, 2006], with higher resolution attainable via the use of model-dependent scaling techniques [*Landerer and Swenson*, 2012].

In this study, we use Release 5 data produced by the Center for Space Research (CSR). CSR gravity fields are provided as spherical harmonic coefficient sets complete to degree and order 60. The gravity field coefficients contain both random and systematic errors, so before the data are converted to mass (in units of millimeter equivalent water thickness) and gridded, a two-step filtering process is applied. Systematic errors, identified by correlations between coefficients, are removed using the filter described by *Swenson and Wahr* [2006], while the random error component, which increases as a function of decreasing wavelength, is reduced by smoothing the data with a Gaussian filter with a half width corresponding to 250 km [*Wahr et al.*, 1998].

2.3. FLUXNET-MTE Latent Heat Flux Data

The FLUXNET-MTE data set [*Jung et al.*, 2009] provides global, gridded estimates of surface to atmosphere fluxes of sensible heat, latent heat, and carbon with a spatial resolution of 0.5° longitude × 0.5° latitude and a monthly temporal resolution. The data used here cover the time period 1982 to 2011. FLUXNET-MTE uses a machine-learning algorithm (Model Tree Ensemble, or MTE) to estimate surface-atmosphere fluxes from a suite of explanatory variables describing meteorological and land surface conditions [*Jung et al.*, 2011]. The MTE was trained using eddy covariance observations from individual FLUXNET facilities and then applied at the global scale. *Bonan et al.* [2011] previously used the FLUXNET-MTE data set to evaluate CLM simulations of gross primary productivity and ET globally and identified errors in both model structure and parameter values in the vegetation biogeophysical model components. In this study, we convert the FLUXNET-MTE latent heat flux estimates to a mass flux (i.e., evapotranspiration or ET) by multiplying by the inverse of the latent heat of vaporization.

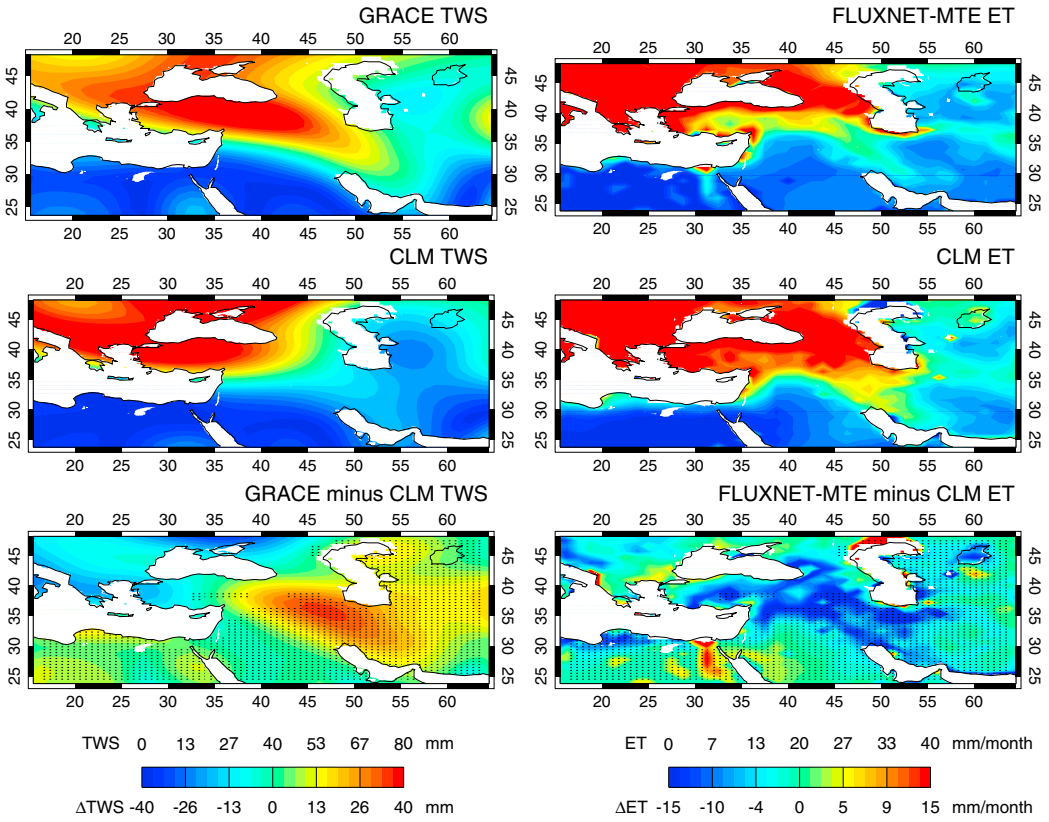

Figure 1. Mean annual amplitude of TWS from (top left) GRACE and (middle left) CLM (mm). Mean annual ET from (top right) FLUXNET-MTE and (middle right) CLM (mm/month). (bottom row) Differences are shown. Stippling indicates areas having greater than 25% bare soil in the CLM surface data set.

3. Assessing TWS and ET Simulated by CLM

Figure 1 shows maps of the annual amplitude of total water storage and annual mean evapotranspiration in the region bounded by 15°–60°E and 15°–50°N. To avoid discrepancies due to a mismatch in spatial resolution, the CLM TWS spatial resolution has been matched to that of the GRACE TWS data by applying the same filters used in the GRACE data processing.

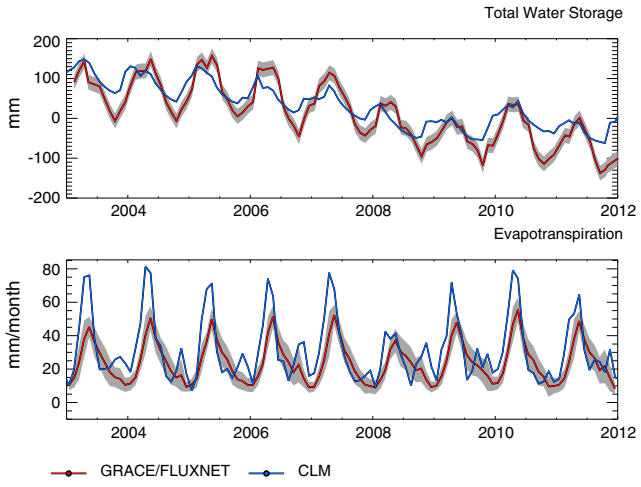

Figure 2. Regional time series centered at 48°E/36°N. (top) Monthly total water storage (mm) from GRACE (red line) and CLM (blue line). (bottom) Monthly total ET mm/month from FLUXNET-MTE (red line) and CLM (blue line). Gray shading indicates 1 standard deviation uncertainty bounds.

The GRACE TWS map (Figure 1, top left) shows an area having a large seasonal cycle centered around 37°E/38°N and extending to the southeast as far as 55°E/28°N, i.e., from Turkey into Iran. In contrast, the area of largest amplitude in the CLM TWS map is confined to a region west of about 45°E and north of about 36°N. Conversely, CLM overestimates ET in Turkey and Iran (Figure 1, right column).

Figure 2 shows time series of TWS and ET for a region centered in NW Iran (48°E/36°N). Both the observed and modeled TWS time series show a long-period decline in total water

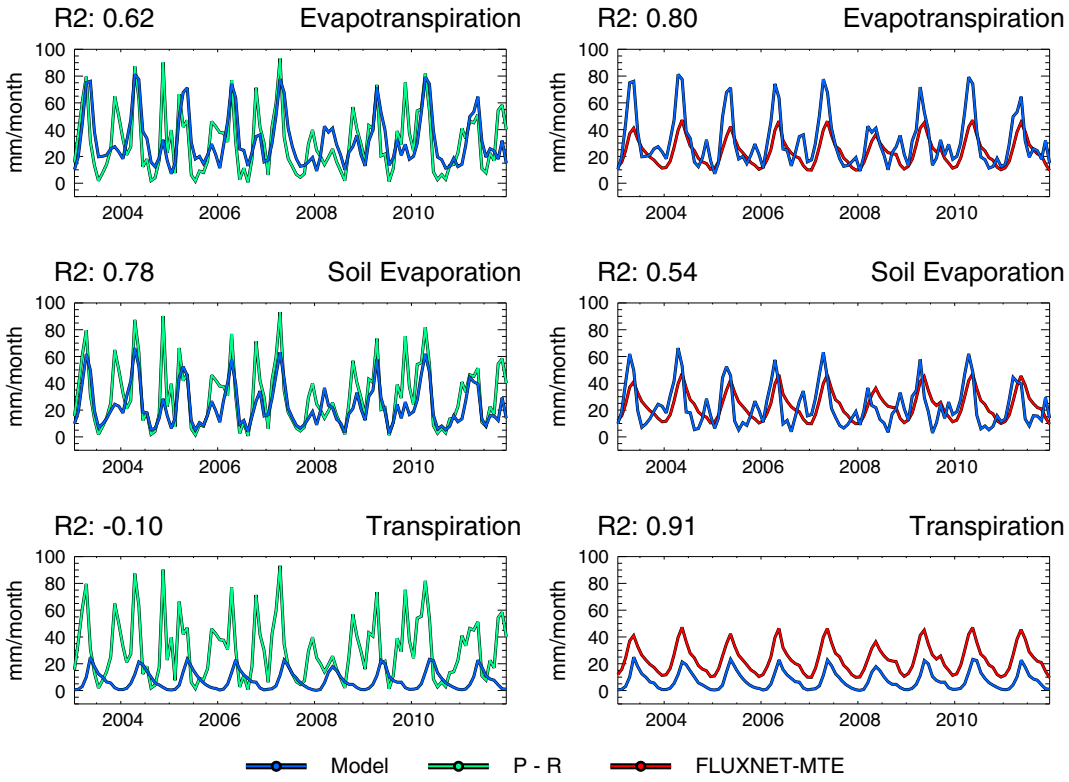

Figure 3. CLM simulated evaporative fluxes ((top row) total ET, (middle row) soil evaporation, (bottom row) transpiration) compared to (left column) CLM precipitation minus runoff and (right column) FLUXNET-MTE ET. R^2 values of each pair of time series are shown at the top left of each panel.

storage, but the seasonal cycle of GRACE TWS is roughly twice as large as that of the CLM TWS. The mean annual amplitudes, obtained by simultaneously fitting an annual sine, annual cosine, mean, and linear trend, are 60.6 ±2.7 mm for GRACE and 29.0 for CLM.

The weak annual amplitude of CLM TWS is related to problems with the CLM ET simulation, which is generally larger, and the maximum values occur earlier than in FLUXNET-MTE. The mean seasonal amplitudes are 18.0 ± 1.1 mm/month and 25.8 mm/month for FLUXNET-MTE and CLM, respectively. The corresponding mean annual ET values are 23.2 ± 0.7 mm/month and 32.1 mm/month.

Figure 3 shows the relative contributions of soil evaporation and transpiration to total evapotranspiration (direct evaporation from the canopy is negligible in this region). Figure 3 (left column) compares the monthly flux of precipitation minus runoff from CLM (*P-R*, green line) to the CLM components of ET (blue lines): total evapotranspiration (top), soil evaporation (middle), and transpiration (bottom). Visually, it is apparent that soil evaporation and *P-R* are highly correlated ($R^2 = 0.78$), while transpiration and *P-R* are uncorrelated ($R^2 = -0.10$). In comparison, the correlation between *P-R* and FLUXNET-MTE ET has an R^2 of 0.14.

In Figure 3 (right column), the CLM components of ET are compared to the FLUXNET-MTE total ET estimates. The CLM soil evaporation time series is moderately correlated with the FLUXNET-MTE ET time series ($R^2 = 0.54$), while the CLM transpiration time series and the observed ET time series are very highly correlated ($R^2 = 0.91$). Furthermore, soil evaporation is the largest component of the total CLM ET, and at some times is larger than the observed total ET.

4. Soil Resistance Parameterization

4.1. Standard CLM Soil Resistance

The tight coupling between the moisture inputs to the soil (*P-R*) and the soil evaporation in CLM can be traced to the formulation of the soil resistance to evaporation. CLM4.5 uses a "soil beta" parameterization

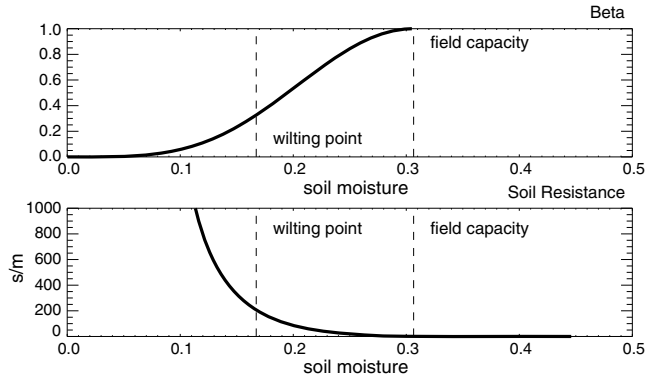

Figure 4. (top) Soil beta factor (β_{soil}) as a function of top layer soil moisture for a soil characterized as 34% sand and 24% clay. (bottom) Equivalent resistance to soil evaporation (s/m). Dashed vertical lines represent field capacity and wilting point soil moisture values.

in which an empirical function that varies from 0 to 1 is used to represent the effect of soil resistance on soil evaporation:

$$E_{soil} = -\rho_{atm} \frac{\beta_{soil}\left(q_{atm} - q_{soil}\right)}{r_{aw}} \quad (1)$$

where E_{soil} is the soil evaporation (mm/s), ρ_{atm} is the density of atmospheric air (kg/m^3), q_{atm} and q_{soil} are the specific humidities of the atmosphere and soil surface (kg/kg), respectively, and r_{aw} is the atmospheric resistance to water vapor transfer (s/m). The soil beta function, which represents the dependence of soil resistance on soil moisture, is

$$\beta_{soil} = \begin{cases} 1 & \theta_{top} \geq \theta_{fc} \text{ or } q_{atm} > q_{soil}, \\ 0.25\left[1 - cos\left(\pi \frac{\theta_{top}}{\theta_{fc}}\right)\right]^2 & \theta_{top} < \theta_{fc} \end{cases} \quad (2)$$

where θ_{top} is the CLM top layer volumetric soil moisture and θ_{fc} is the field capacity of the top layer [*Sakaguchi and Zeng*, 2009; *Lee and Pielke*, 1992; *Lawrence et al.*, 2011]. For a given value of r_{aw}, an equivalent soil resistance can be obtained from β_{soil} via

$$r_\beta = r_{aw}\left(\frac{1}{\beta_{soil}} - 1\right), \quad (3)$$

which can be used to reexpress equation (1) in terms of resistances:

$$E_{soil} = -\rho_{atm} \frac{\left(q_{atm} - q_{soil}\right)}{r_{aw} + r_\beta}. \quad (4)$$

As an example, Figure 4 shows β_{soil} (top) and the equivalent soil resistance (bottom) as a function of volumetric soil moisture for the CLM soil type at 48°E/36°N, which consists of 34% sand and 24% clay. For this soil, wilting point is approximately 0.17, field capacity is about 0.31, and saturation (i.e., porosity) is about 0.45. As specified by equation (2), β_{soil} is 1 for all soil moisture values above field capacity, and the soil resistance is therefore zero. As drying progresses from field capacity to wilting point, β_{soil} drops to 0.33, equivalent to a resistance of 207 s/m, compared to the prescribed aerodynamic resistance of 100 s/m.

Sakaguchi and Zeng [2009] contend that when soils are relatively moist, it is a combination of surface litter and stable under-canopy air conditions that limit soil evaporation, rather than resistance from the soil matrix. However, in the region examined here, much of the ground surface is bare soil (Figure 1) and the grid cell average leaf area index (LAI) values are generally well below 1. In the region examined in Figures 2 and 3 (48°E/36°N), annual mean LAI is 0.17, with peak values of 0.31. These LAI values imply that vegetation (live or dead) is not the dominant control on soil evaporation, but instead, soil evaporation is controlled by moisture conditions in the soil matrix. Furthermore, while surface litter and under-canopy stability may contribute to soil evaporation limitation, they are likely overestimated in CLM to account for the low soil resistance values predicted by the soil beta function.

Figure 5 shows hourly CLM output for precipitation, soil moisture, soil evaporation, and soil resistance for the grid cell located at 48°E/36°N. Because the effective soil resistances determined by the β_{soil} function are relatively low for soil moisture above wilting point (0.17 for this soil type), soil evaporation remains high between precipitation events. This leads to relatively little infiltration reaching the deeper soil layers, evidenced by the absence of vertical pulses of moisture into the soil after large rain events. For the soil type at this location, field capacity is 0.31, or about 0.69 times saturation. Figure 5 shows that the soil in this grid

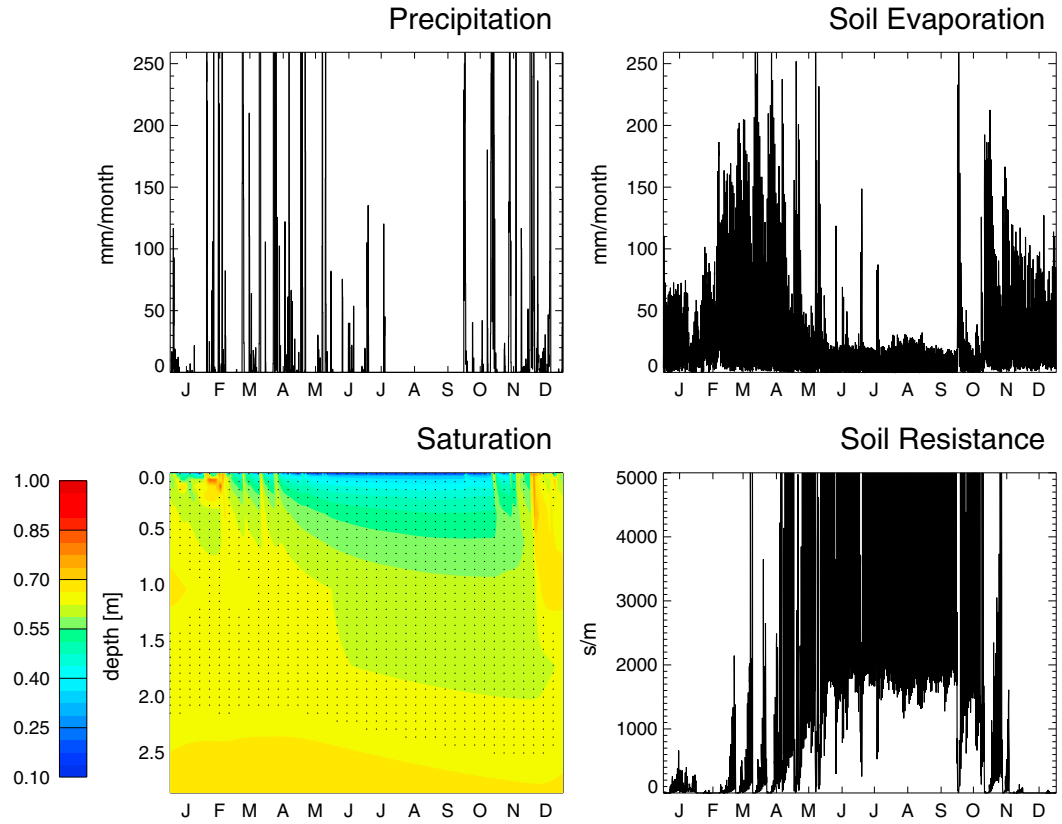

Figure 5. Hourly output of a 1 year CLM simulation for the grid cell located at 48°E/36°N. (top left) Precipitation (mm/month), (top right) soil evaporation (mm/month), (bottom left) soil moisture saturation (stippling indicates values of soil moisture below field capacity), and (bottom right) equivalent soil resistance (s/m). Note that instances of high precipitation, soil evaporation, and soil resistance may be cut off in these plots.

cell is below field capacity for almost all times to a depth of roughly 2 m. Of the few infiltration events that are visible, most of the water is soon returned to the atmosphere, rather than stored deeper in the soil column. The role of the β_{soil} function can be seen in Figure 5 (bottom right). While large values of soil resistance can be observed, these occur only after the soil has dried substantially. Average daytime atmospheric aerodynamic resistances in this simulation are roughly 100 s/m; soil resistances remain below this value until soil moisture is below about 0.19. When soils are moist, soil resistances are quite low (Figure 5), leading to prolonged drying in the simulation.

4.2. Dry Surface Layer Parameterization

To address the shortcomings of the soil evaporative resistance function used in the simulation shown in Figure 5, we have implemented an alternative soil resistance parameterization in CLM. Rather than parameterize the soil resistance directly from the surface layer soil moisture, the alternative method diagnoses the thickness of a dry surface layer and calculates the soil resistance that would result if soil evaporation were controlled by diffusion across the DSL (when it exists). The parameterization therefore focuses on the physical process limiting soil evaporation and can in principle be compared directly to observations of the DSL.

The DSL is parameterized as a function of the top soil layer soil moisture:

$$\mathrm{DSL} = \begin{cases} \Delta z \dfrac{\left(\theta_{\mathrm{dsl0}} - \theta_{\mathrm{top}}\right)}{\left(\theta_{\mathrm{dsl0}} - \theta_{\mathrm{air}}\right)} & \theta_{\mathrm{top}} < \theta_{\mathrm{dsl0}} \\ 0 & \theta_{\mathrm{top}} \geq \theta_{\mathrm{dsl0}}, \end{cases} \tag{5}$$

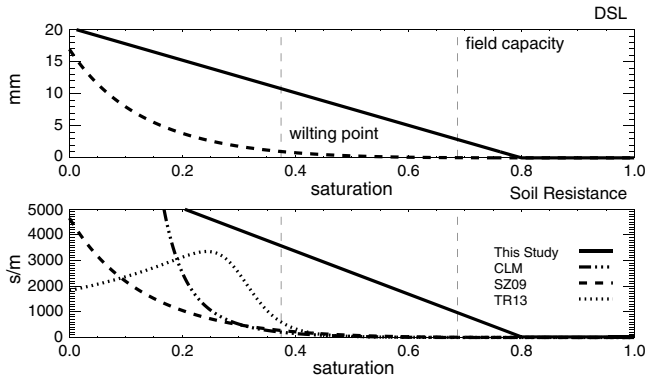

Figure 6. (top) DSL thickness as a function of top layer soil moisture for a soil characterized as 34% sand and 24% clay. (bottom) Resistance to soil evaporation (s/m). Dashed vertical lines represent field capacity and wilting point soil moisture values.

where Δz is a parameter specifying the length scale of the maximum DSL thickness (m), θ_{dsl0} is the moisture value at which the DSL initiates, θ_{top} is the moisture value of the top model soil layer, and θ_{air} is the "air-dry" soil moisture value [*Dingman*, 2002]:

$$\theta_{air} = \Phi \left(\frac{\Psi_{sat}}{\Psi_{air}} \right)^{\frac{1}{b}} . \quad (6)$$

where Ψ_{sat} is the saturated soil matric potential, Ψ_{air} = 1E7 mm is the air-dry matric potential, and b is the soil water characteristic parameter. In this study, Δz is specified as 15 mm, based on the observed range of maximum DSL thicknesses of 10–30 mm [*van de Griend and Owe*, 1994; *Goss and Madliger*, 2007; *Smits et al.*, 2012], and θ_{dsl0} is specified as a constant fraction of a saturated soil:

$$\theta_{dsl0} = K\Phi , \quad (7)$$

where Φ is the porosity; in this study, $K = 0.8$. This value of K was calibrated via the metric of the simulation's performance at reproducing the GRACE TWS seasonal cycle amplitude globally. For some soil types, especially sandier soils, the choice to define θ_{dsl0} as a function of porosity rather than field capacity implies that a DSL can initiate when the average top layer soil moisture is above field capacity.

Equation (5) states that as drying progresses from saturation, a dry surface layer develops only after the soil moisture falls below a threshold, given by θ_{dsl0} . The presence of a threshold in equation (5) is motivated by *Shokri and Or* [2011], who observed a discrete jump in connectivity of liquid menisci as the DSL formed. Continued drying results in formation of a dry surface layer, whose thickness is determined by the amount of water removed from the soil, scaled by the amount of water required to reduce the soil moisture in the DSL to its air-dry value.

After the dry surface layer thickness has been determined, the soil resistance to evaporation follows from

$$R_{soil} = \frac{DSL}{D_v \tau} . \quad (8)$$

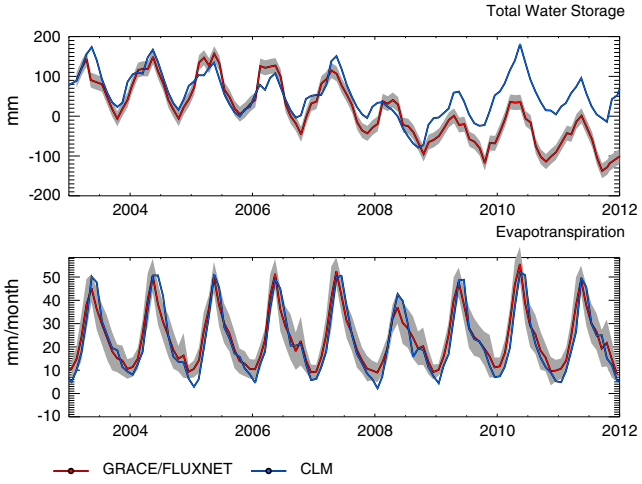

Figure 7. Like Figure 2 except that CLM simulation uses DSL-based soil resistance parameterization.

where D_v is the molecular diffusivity of water vapor in air (m^2/s), and τ describes the tortuosity of the vapor flow paths through the soil matrix [*Deol et al.*, 2012; *Yamanaka et al.*, 1997]. The expression for τ used here was taken from *Moldrup et al.* [2003]

$$\tau = \Phi_{air}^2 \left(\frac{\Phi_{air}}{\Phi} \right)^{\frac{3}{b}} . \quad (9)$$

where $\Phi_{air} = \Phi - \theta_{air}$ is the air-filled pore space.

Figure 6 shows the relationships between DSL thickness, soil resistance, and top layer soil moisture for a soil defined as being 34% sand and 24% clay. Figure 6 (top) shows the DSL thickness obtained using equation (5)

Table 1. Comparison of Seasonal Amplitudes and Annual Mean Values for Observations and CLM Simulations for the Region Centered on (48°E/36°N)

	Regional Statistics		
	TWS Seasonal (mm)	ET Seasonal (mm/month)	ET Annual Mean (mm/month)
Observed	60.6 ± 2.7	18.0 ± 1.1	23.2 ± 0.7
Control	29.0	25.8	32.1
Experiment	48.8	21.0	23.1

(solid line) as well as the DSL described by *Sakaguchi and Zeng* [2009] (dashed line). Figure 6 (bottom) compares the soil resistances obtained from equation (8) (solid line), the standard CLM soil beta function (dash-dotted line), the *Sakaguchi and Zeng* [2009] DSL function (dashed line), and the *Tang and Riley* [2013] function (dotted line). Relative to the new parameterization, the other soil resistances are significantly lower for all values of soil moisture above approximately 20% saturation.

5. Results

Figure 7 shows times series of TWS and ET for the region centered in NW Iran (48°E/36°N). The GRACE and FLUXNET-MTE time series are the same as those in Figure 2, while the CLM time series are from a simulation using the DSL-based soil resistance expression. From Figure 7, one can see that the modified simulation performs better against both metrics. As before, the amplitude of the best fitting mean annual cycle for the GRACE TWS time series is 60.6 ± 2.7 mm, while the CLM amplitude has increased from 29.0 for the standard CLM to 48.8 in the modified CLM (Table 1). This increase is the result of a reduction of the CLM ET seasonal amplitude, from 25.8 mm/month to 21.0 mm/month; the mean FLUXNET-MTE seasonal amplitude is 18.0 ± 1.1 mm/month. This reduction is also reflected in the annual mean ET , which has been reduced from 32.1 mm/month in the original simulation to 23.1 mm/month in the new simulation; the latter value agrees closely with the FLUXNET-MTE annual mean ET value of 23.2 ± 0.7 mm/month.

The divergence of the two TWS time series after 2008 was explained by *Joodaki et al.* [2014] as the result of anthropogenic groundwater withdrawal. GRACE TWS is sensitive to all mass changes in the region and

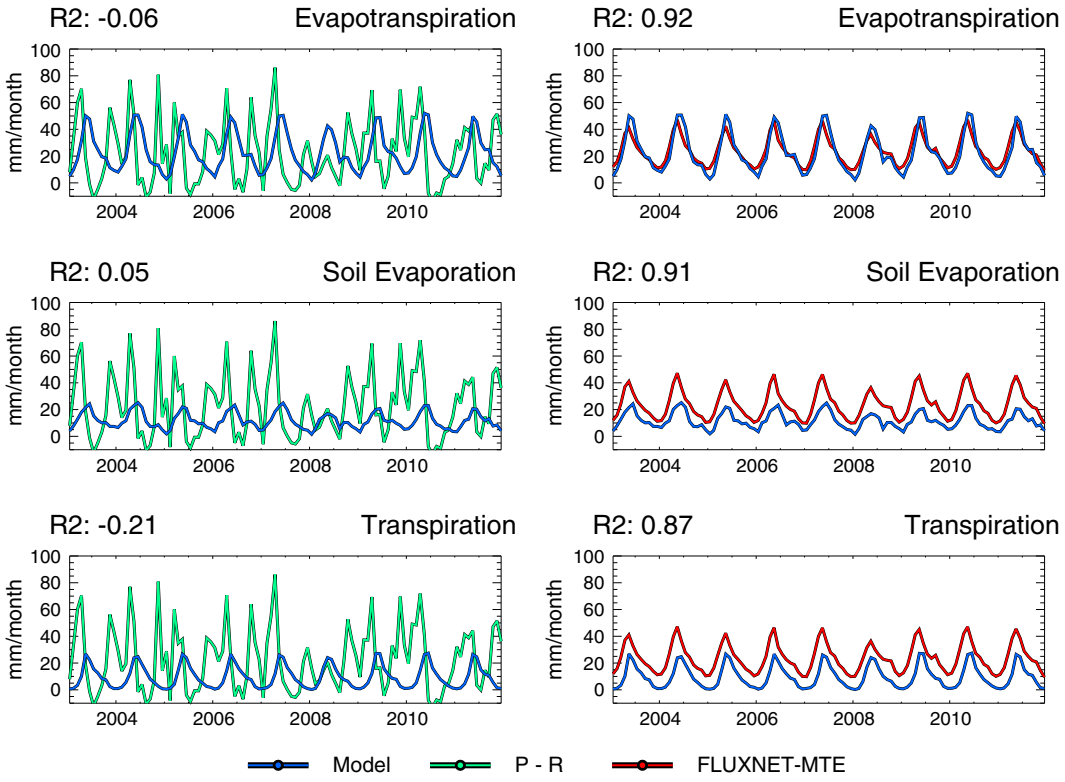

Figure 8. Like Figure 3 except that CLM simulation uses DSL-based soil resistance parameterization.

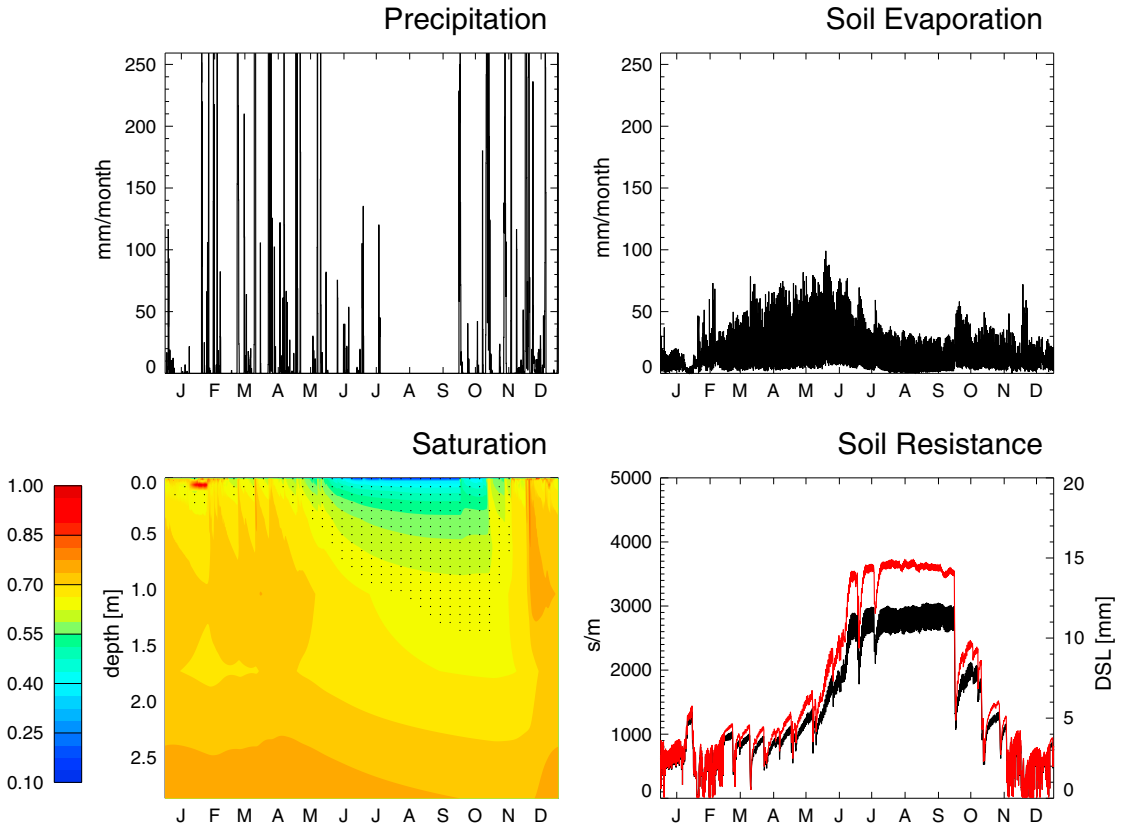

Figure 9. Hourly output of a 1 year CLM simulation using the DSL-based soil resistance for the grid cell located at 48°E/36°N. (top left) Precipitation (mm/month), (top right) soil evaporation (mm/month), (bottom left) soil moisture saturation, and (bottom right) equivalent soil resistance (s/m) (black line, left *y* axis) and DSL thickness (mm) (red line, right *y* axis).

therefore observes the decline in water storage due to groundwater irrigation. In contrast, CLM responds to climate variability through the atmospheric forcing used to drive the simulation but currently does not simulate anthropogenic groundwater withdrawal. Although the CLM simulation does not predict the post-2008 decline captured by the GRACE TWS measurements, this has limited impact on simulated surface fluxes and near-surface soil moisture conditions because the simulated water table is relatively deep (~8 m), and groundwater-soil moisture interactions are primarily in the form of recharge to the aquifer.

The relative impact of the DSL-based soil resistance parameterization on the components of ET can be seen in Figure 8. Comparison of Figures 8 and 3 reveals that the change in total ET in the new simulation is primarily due to changes in soil evaporation. The strong correlation between soil evaporation and *P-R* (R^2 = 0.78, Figure 3 (left column)) is largely gone in the new simulation (R^2 = 0.07, Figure 8 (middle left)). Instead, the soil evaporation time series varies more smoothly and is in phase with the FLUXNET-MTE ET time series (R^2 = 0.90). Moreover, CLM soil evaporation values are always less than the FLUXNET-MTE total ET values. Transpiration has not changed significantly between the two simulations.

Figure 9 shows the effect of the DSL-based soil resistance parameterization on infiltration and soil moisture. Relative to the original simulation, soil evaporation in the new simulation is reduced, and the peak values are shifted later in the year. More water that infiltrates subsequently penetrates to depth, leading to overall wetter soil conditions, especially during the winter season when soil moisture values are near field capacity. Near-surface soil moisture conditions are similar during the summer, although the drying front penetrates less deeply in the new simulation. Soil resistances are less variable, and while they drop during precipitation events, they grow rapidly enough afterward to prevent prolonged drying of the soil. Simulated DSL thickness at this location varies between 0 and 15 mm. This maximum DSL thickness is comparable to laboratory and field studies, where maximum DSL thickness of 10–30 mm have been observed [*van de Griend and Owe*, 1994; *Goss and Madliger*, 2007; *Smits et al.*, 2012].

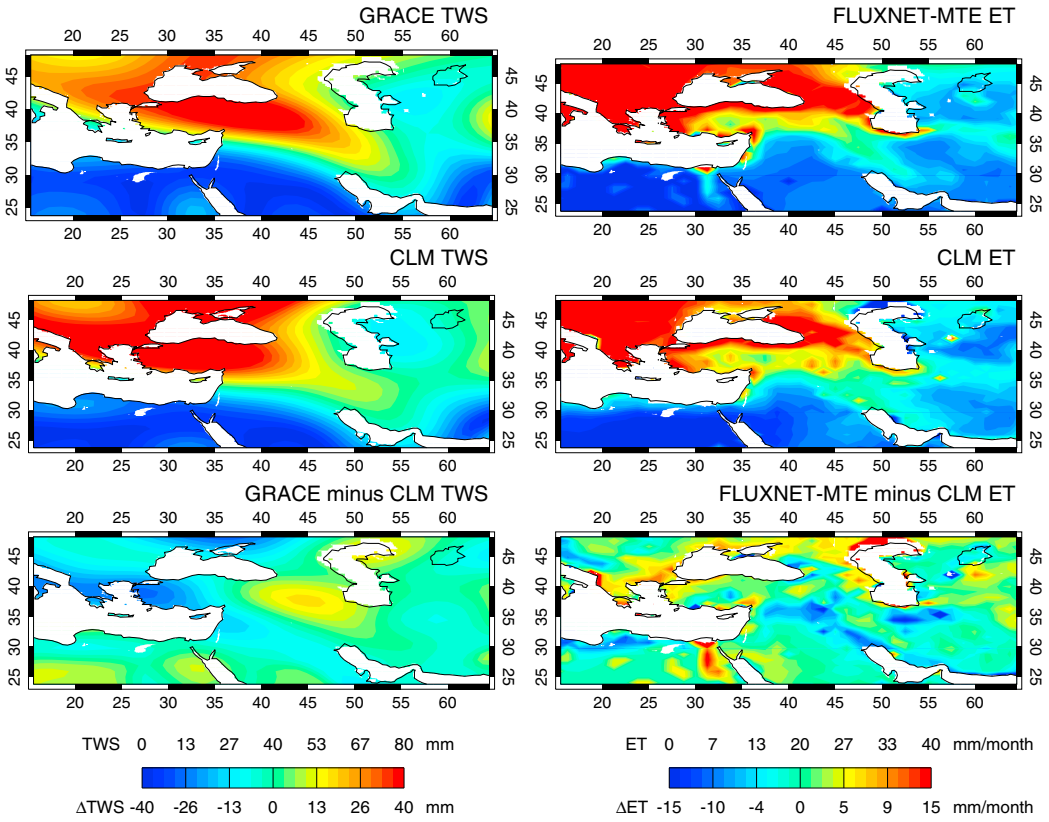

Figure 10. Like Figure 1 except that CLM simulation uses DSL-based soil resistance parameterization.

The new simulation shows similar improvements relative to the metrics of GRACE TWS and FLUXNET-MTE ET throughout the region shown in Figure 1. Figure 10 shows maps of the mean annual amplitude of TWS and mean annual ET. The area of large annual amplitude TWS in the GRACE TWS map that extends from Turkey to Iran is well reproduced in the CLM simulation that uses the DSL-based soil resistance. At the same time, the mean annual ET values in that region are generally reduced, agreeing more closely with the FLUXNET-MTE values.

When averaged over all global semiarid regions (an area of 28.0×10^6 km^2), the CLM mean annual amplitude of TWS has increased from 26.3 mm to 32.5 mm; the averaged GRACE mean annual amplitude is 32.2 ± 2.1 mm (Table 2). The RMS difference decreases slightly, from 18.8 mm to 18.2 mm; the average monthly GRACE TWS errors are estimated to be 15.8 mm. CLM mean annual ET, when averaged over all semiarid regions, decreases from 27.8 mm/month to 23.5 mm/month; FLUXNET-MTE mean annual ET for these regions is 21.1 ± 0.9 mm/month. The seasonal amplitude of CLM ET also decreases, from 23.3 mm/month to 18.3 mm/month compared to 14.9 ± 1.1 mm/month for FLUXNET-MTE. The ET RMS difference decreases from 13.7 mm/month to 8.3 mm/month; the average monthly FLUXNET-MTE uncertainty is 8.7 mm/month.

Table 2. Comparison of Seasonal Amplitudes and Annual Mean Values for Observations and CLM Simulations Averaged Globally

	Global Statistics		
	TWS Seasonal (mm)	ET Seasonal (mm/month)	ET Annual Mean (mm/month)
Observed	32.2 ± 2.1	14.9 ± 1.1	21.1 ± 0.9
Control	26.3	23.3	27.8
Experiment	32.5	18.3	23.5

6. Discussion

6.1. Benefits and Challenges of Parameterizing the DSL

The results presented in the previous section demonstrate that the coupled ET and TWS biases can be greatly reduced by increasing the soil resistance to evaporation. Rather than directly parameterize the soil resistance as a function of soil moisture, as is commonly done, we parameterize the thickness of a dry surface layer, from which soil resistance is calculated. One motivation for this choice is that observational studies of bare soil evaporation indicate that the process of the formation of the DSL, and its evolution with time provide fundamental control on the magnitude of soil evaporation as drying progresses [*Kondo and Saigusa*, 1994; *Yamanaka et al.*, 1997; *Liu et al.*, 2005; *Goss and Madliger*, 2007; *Shokri and Or*, 2011; *Deol et al.*, 2012; *Smits et al.*, 2012].

While discussed qualitatively decades ago [e.g., *Philip*, 1957], it is only recently that high-resolution quantitative measurements of the DSL thickness have been reported [*Deol et al.*, 2012; *Xiao et al.*, 2012]. This may help explain why typically soil resistance has been parameterized rather than the DSL directly. A DSL-based soil resistance parameterization was presented by *Sakaguchi and Zeng* [2009], but without observational constraints, the soil resistances resulting from their formulation were too low, and the effect could not be discerned from that of the β_{soil} function. *Tang and Riley* [2013] proposed a soil resistance parameterization based on liquid and vapor diffusion across a layer of fixed thickness, but the resulting soil resistances are smaller than those predicted by the β_{soil} function, except for very dry soils, and a simulation implementing their parameterization does not show improvement relative to GRACE TWS and FLUXNET-MTE ET.

Another motivation for parameterizing the DSL directly is the need for a soil resistance formulation that can be applied globally. Most soil resistance parameterizations based on laboratory or field studies were developed for a specific soil type or contain limited soil-type dependence (i.e., via porosity alone). In the DSL-based parameterization, information on soil type is contained in the DSL equation (equation (5)), as well as the equation for the soil resistance (equation (8)), which explicitly represents the effects of soil type through the tortuosity term, τ, providing a more comprehensive description of the effect of soil type on the soil resistance [*Moldrup et al.*, 2003].

The surface energy balance was modified through changes in the latent heat flux, but the direct effect of the DSL on the sensible heat flux was not included. Explicitly accounting for the thermal properties of the dry surface layer would tend to increase the diurnal amplitude of surface soil temperature, due to decreased thermal conductivity and heat capacity. Currently, CLM includes a tuned parameter that modifies the heat capacity of the top soil layer (through adjustment of the layer thickness) to increase the diurnal amplitude of surface temperature. Subsequent research will examine whether adding the thermal properties of the dry surface layer can eliminate the need for the adjustment of the top soil layer's heat capacity.

The DSL parameterization presented here is not based on direct observations, but on the basic characteristics of DSL evolution as described in field and laboratory studies. In a sensitivity analysis, we found that increasing Δz by 5 mm led to an 11% decrease in annually averaged soil evaporation, while decreasing Δz by 5 mm led to an 11% increase in annually averaged soil evaporation; increasing K by 0.1 led to a 17% decrease in annual soil evaporation, while decreasing K by 0.1 led to a 28% increase in annual soil evaporation (relative to the default values). Future research will use high-resolution observations of the evolution of the DSL as a function of soil moisture and soil type to inform improvements to the functional form and parameter values of the DSL parameterization. A necessary part of such work will include modeling studies examining the role of model vertical resolution and structure (e.g., single versus multiphase transport), and especially the correspondence between modeled and observed soil moisture values.

6.2. Land-Atmosphere Interactions

The ability to effectively model soil evaporation is important for understanding the role of soil moisture memory in land-atmosphere interactions [*Lawrence et al.*, 2007; *Seneviratne et al.*, 2006]. In the standard CLM, storage of soil moisture in semiarid regions plays a limited role in the exchange of moisture between the land and atmosphere; evaporation coincides with precipitation, which is almost immediately returned to the atmosphere (Figure 5). In contrast, the DSL-based soil resistance reduces evaporation when soils are moist but increases evaporation later in the season due to higher soil moisture storage (Figure 6). This implies that the standard CLM may underestimate the effect of soil moisture memory on land-atmosphere fluxes.

Realistically representing the differences in land-atmosphere interactions between vegetated and nonvegetated soils is also important for simulating the effects of future land cover change. A land cover sensitivity study in which all CLM vegetation is replaced with bare soils leads to a simulation in which global total ET actually increases relative to the control simulation (P. Lawrence, personal communication, 2013). A similar sensitivity study using the DSL-based soil resistance shows an overall decrease in global ET and an increase in runoff when vegetation is replaced by bare soil. The latter result is more consistent with the hypothesis that plant physiology (stomata and a vascular system) evolved to overcome the barrier to subsurface soil moisture caused by the drying of the surface soil layer [*Berry et al.*, 2010].

6.3. ET Partitioning

Some recent studies point toward a transpiration-dominated global ET budget. *Jasechko et al.* [2013], based on a stable isotope analysis of large lakes, concluded that transpiration contributed 80–90% of the globally averaged flux of ET. *Miralles et al.* [2011] used a satellite data-forced model to arrive at a similar value (80%) for the global transpiration contribution. While these estimates are subject to considerable uncertainty [e.g., *Coenders-Gerrits et al.*, 2014], they suggest that the current CLM transpiration fraction (48%) may be too low. Applying the DSL-based soil resistance, parameterization in CLM changes both the simulated total ET and its partitioning. Transpiration increases and soil evaporation decreases, leading to a change in the fractional contribution of transpiration to the CLM ET budget from 48% to 57% (soil evaporation drops from 33% to 22%; the remaining contribution coming from canopy evaporation).

6.4. Summary

There is a large spread in global ET estimates [*Jiménez et al.*, 2011], and this implies even greater uncertainty exists in regional ET estimates. However, the use of multiple independent data sets (GRACE and FLUXNET-MTE) greatly increases the ability to constrain model performance [*Luo et al.*, 2012]. Despite the absence of direct observations of soil resistance or soil evaporation at the spatial scales of a typical global CLM simulation, the effects of modifying the soil resistance parameterization can be assessed by focusing on a broad region in which soil evaporation is a major component of the ET budget. In our study region, biases relative to FLUXNET-MTE ET and GRACE TWS observations are consistent with a bias in soil evaporation toward values that are too large and too responsive to precipitation inputs. Changes in simulated soil evaporation due to the DSL-based soil resistance formulation are clearly manifested in total ET. Furthermore, we have shown that the bias reduction in ET relative to the FLUXNET-MTE data is corroborated by the concurrent bias reduction relative to the independently observed GRACE TWS observations. This aggregate metric of model improvement provides a stronger confirmation of the need to reduce the bare soil evaporation in CLM than either data set would alone. The DSL parameterization introduced here represents a more mechanistic description of soil evaporation and is a starting point from which improvements can be made with additional observational and experimental studies of DSL evolution in a variety of soil types and climatic conditions.

Acknowledgments

This research was supported by the Regional and Global Climate Modeling Program (RGCM) of the U.S. Department of Energy's Office of Science (BER), Cooperative Agreement DE-FC02-97ER62402. We wish to thank Kathleen Smits and Peter Lawrence for conversations that greatly improved this research. The Associate Editor and three reviewers provided valuable input that helped shape the final manuscript. Source code for the Community Land Model is available from http://www.cesm.ucar.edu/models/cesm1.0/. GRACE data can be obtained from ftp://podaac.jpl.nasa.gov/allData/grace/L2/CSR/RL05/. FLUXNET-MTE data can be obtained from http://www.bgc-jena.mpg.de/geodb/projects/Home.php.

References

Alton, P., R. Fisher, S. Los, and M. Williams (2009), Simulations of global evapotranspiration using semiempirical and mechanistic schemes of plant hydrology, *Global Biogeochem. Cycles*, *23*, GB4023, doi:10.1029/2009GB003540.

Berry, J. A., D. J. Beerling, and P. J. Franks (2010), Stomata: Key players in the earth system, past and present, *Curr. Opin. Plant Biol.*, *13*, 223–240.

Bonan, G. B., P. J. Lawrence, K. W. Oleson, S. Levis, M. Jung, M. Reichstein, D. M. Lawrence, and S. C. Swenson (2011), Improving canopy processes in the Community Land Model version 4 (CLM4) using global flux fields empirically inferred from FLUXNET data, *J. Geophys. Res.*, *116*, G02014, doi:10.1029/2010JG001593.

Coenders-Gerrits, A. M. J., R. J. van der Ent, T. A. Bogaard, L. Wang-Erlandsson, M. Hrachowitz, and H. H. G. Savenije (2014), Uncertainties in transpiration estimates, *Nature*, *506*, E1–E2, doi:10.1038/nature12925.

Deol, P., J. Heitman, A. Amoozegar, T. Ren, and R. Horton (2012), Quantifying nonisothermal subsurface soil water evaporation, *Water Resour. Res.*, *48*, W11503, doi:10.1029/2012WR012516.

Dingman, S. L. (2002), *Physical Hydrology,* 2nd ed., Prentice-Hall, Saddle River, N. J.

Gent, P. R., et al. (2011), The community climate system model version 4, *J. Clim.*, *24*, 4973–91.

Goss, K. U., and M. Madliger (2007), Estimation of water transport based on in situ measurements of relative humidity and temperature in a dry Tanzanian soil, *Water Resour. Res.*, *43*, W05433, doi:10.1029/2006WR005197.

Haddeland, I., et al. (2011), Multimodel estimate of the global terrestrial water balance: Setup and first results, *J. Hydrometeorol.*, *12*, 869–884, doi:10.1175/2011JHM1324.1.

Huffman, G. J., R. F. Adler, P. Arkin, A. Chang, R. Ferraro, A. Gruber, J. Janowiak, A. McNab, B. Rudolf, and U. Schneider (1997), The Global Precipitation Climatology Project (GPCP) combined precipitation dataset, *Bull. Am. Meteorol. Soc.*, *78*(1), 5–20.

Hurrell, J. W., et al. (2013), The Community Earth System Model: A framework for collaborative research, *Bull. Am. Meteorol. Soc.*, *94*(9), 1339–1360, doi:10.1175/BAMS-D-12-00121.1.

Jasechko, S., Z. D. Sharp, J. J. Gibson, S. J. Birks, Y. Yi, and P. J. Fawcett (2013), Terrestrial water fluxes dominated by transpiration, *Nature*, *496*(7445), 347–350.

Jiménez, C., et al. (2011), Global intercomparison of 12 land surface heat flux estimates, *J. Geophys. Res.*, *116*, D02102, doi:10.1029/2010JD014545.

Joodaki, G., J. Wahr, and S. Swenson (2014), Estimating the human contribution to groundwater depletion in the Middle East, from GRACE data, land surface models, and well observations, *Water Resour. Res.*, *50*, 2679–2692, doi:10.1002/2013WR014633.

Jung, M., et al. (2009), Towards global empirical upscaling of FLUXNET eddy covariance observations: Validation of a model tree ensemble approach using a biosphere model, *Biogeosciences*, *6*, 2001–2013, doi:10.5194/bg-6-2001-2009.

Jung, M., et al. (2011), Global patterns of land-atmosphere fluxes of carbon dioxide, latent heat, and sensible heat derived from eddy covariance, satellite, and meteorological observations, *J. Geophys. Res.*, *116*, G00J07, doi:10.1029/2010JG001566.

Kondo, J., and N. Saigusa (1994), Modeling the evaporation from bare soil with a formula for vaporization in the soil pores, *J. Meteorol. Soc. Jpn.*, *72*, 413–421.

Kondo, J., N. Saigusa, and T. Sato (1990), A parameterization of evaporation from bare soil surfaces, *J. Appl. Meteorol.*, *29*, 385–389.

Landerer, F. W., and S. C. Swenson (2012), Accuracy of scaled GRACE terrestrial water storage estimates, *Water Resour. Res.*, *48*, W04531, doi:10.1029/2011WR011453.

Lawrence, D. M., P. E. Thornton, K. W. Oleson, and G. B. Bonan (2007), The partitioning of evapotranspiration into transpiration, soil evaporation, and canopy evaporation in a GCM: Impacts on land-atmosphere interaction, *J. Hydrometeorol.*, *8*, 862–880.

Lawrence, D. M., et al. (2011), Parameterization improvements and functional and structural advances in version 4 of the Community Land Model, *J. Adv. Model. Earth Syst.*, *3*, M03001, doi:10.1029/2011MS000045.

Lawrence, D. M., K. W. Oleson, M. G. Flanner, C. G. Fletcher, P. J. Lawrence, S. Levis, S. C. Swenson, and G. B. Bonan (2012), The CCSM4 land simulation, 1850–2005: Assessment of surface climate and new capabilities, *J. Clim.*, *25*, 2240–2260, doi:10.1175/JCLI-D-11-00103.1.

Lee, T. J., and R. A. Pielke (1992), Estimating the soil surface specific humidity, *J. Appl. Meteorol.*, *31*, 480–484, doi:10.1175/1520-0450.

Liu, B. C., W. Liu, and S. W. Peng (2005), Study of heat and moisture transfer in soil with a dry surface layer, *Int. J. Heat Mass Transfer*, *48*, 4579–4589.

Luo, Y. Q., et al. (2012), A framework for benchmarking land models, *Biogeosciences*, *9*(10), 3857–3874, doi:10.5194/bg-9-3857-2012.

Miralles, D. G., R. A. M. de Jeu, J. H. Gash, T. R. H. Holmes, and A. J. Dolman (2011), Magnitude and variability of land evaporation and its components at the global scale, *Hydrol. Earth Syst. Sci.*, *15*, 967–981, doi:10.5194/hess-15-967-2011.

Moldrup, P., T. Olesen, T. Komatsu, S. Yoshikawa, P. Schjonning, and D. E. Rolston (2003), Modeling diffusion and reaction in soils: X. A unifying model for solute and gas diffusivity in unsaturated soil, *Soil Sci.*, *168*, 321–337, doi:10.1097/00010694-200305000-00002.

Oleson, K. W., et al. (2013), Technical description of version 4.5 of the Community Land Model (CLM), *NCAR Tech. Note NCAR/TN-503+STR*, pp. 422, Natl. Cent. for Atmos. Res., Boulder, Colo., doi:10.5065/D6RR1W7M.

Philip, J. R. (1957), Evaporation, and moisture and heat fields in the soil, *J. Meteorol.*, *14*, 354–366.

Sakaguchi, K., and X. Zeng (2009), Effects of soil wetness, plant litter, and under-canopy atmospheric stability on ground evaporation in the Community Land Model (CLM3. 5), *J. Geophys. Res.*, *114*, D01107, doi:10.1029/2008JD010834.

Sellers, P. J., M. D. Heiser, and F. G. Hall (1992), Relations between surface conductance and spectral vegetation indexes at intermediate (100 m^2 to 15 km^2) length scales, *J. Geophys. Res.*, *97*, 19,033–19,059.

Seneviratne, S. I., et al. (2006), Soil moisture memory in AGCM simulations: Analysis of Global Land-Atmosphere Coupling Experiment (GLACE) data, *J. Hydrometeorol.*, *7*, 1090–1112.

Shokri, N., and D. Or (2011), What determines drying rates at the onset of diffusion controlled stage-2 evaporation from porous media?, *Water Resour. Res.*, *47*, W09513, doi:10.1029/2010WR010284.

Shokri, N., P. Lehmann, and D. Or (2009), Critical evaluation of enhancement factors for vapor transport through unsaturated porous media, *Water Resour. Res.*, *45*, W10433, doi:10.1029/2009WR007769.

Smits, K. M., V. V. Ngo, A. Cihan, T. Sakaki, and T. H. Illangasekare (2012), An evaluation of models of bare soil evaporation formulated with different land surface boundary conditions and assumptions, *Water Resour. Res.*, *48*, W12526, doi:10.1029/2012WR012113.

Swenson, S., and J. Wahr (2006), Post-processing removal of correlated errors in GRACE data, *Geophys. Res. Lett.*, *33*(8), L08402, doi:10.1029/2005GL025285.

Tapley, B. D., S. Bettadpur, M. Watkins, and C. Reigber (2004), The gravity recovery and climate experiment: Mission overview and early results, *Geophys. Res. Lett.*, *31*, L09607, doi:10.1029/2004GL019920.

Tang, J. Y., and W. J. Riley (2013), A new top boundary condition for modeling surface diffusive exchange of a generic volatile tracer: Theoretical analysis and application to soil evaporation, *Hydrol. Earth Syst. Sci.*, *17*, 873–893, doi:10.5194/hess-17-873-2013.

van de Griend, A. A., and M. Owe (1994), Bare soil surface-resistance to evaporation by vapor diffusion under semiarid conditions, *Water Resour. Res.*, *30*, 181–188.

Viovy, N. (2013), *CRUNCEP Data Set V5*. [Available at http://dods.ipsl.jussieu.fr/igcmg/IGCM/BC/OOL/OL/CRU-NCEP/, accessed 2013-8-5.]

Wahr, J., M. Molenaar, and F. Bryan (1998), Time variability of the Earth's gravity field: Hydrological and oceanic effects and their possible detection using GRACE, *J. Geophys. Res.*, *103*(B12), 30,205–30,229.

Wahr, J., S. Swenson, and I. Velicogna (2006), The accuracy of GRACE mass estimates, *Geophys. Res. Lett.*, *33*, L06401, doi:10.1029/2005GL025305.

Xiao, Z., S. Lu, J. Heitman, R. Horton, and T. Ren (2012), Measuring subsurface soil-water evaporation with an improved heat-pulse probe, *Soil Sci. Soc. Am. J.*, *76*, 876–879.

Yamanaka, T., A. Takeda, and F. Sugita (1997), A modified surface-resistance approach for representing bare-soil evaporation: Wind tunnel experiments under various atmospheric conditions, *Water Resour. Res.*, *33*, 2117–2128.